Journal of Marine Science and Technology

Volume 28 | Issue 6 Article 13

Internal Force Evaluation of a Submerged Floating Pipeline Under Irregular Waves

Deokhee Won
Coastal & Ocean Engineering Division, Korea Institute of Ocean Science and Technology, Busan, Korea

Jihye Seo
Coastal & Ocean Engineering Division, Korea Institute of Ocean Science and Technology, Busan, Korea.

Jong Sup Park
Department of Civil Engineering, Sangmyung University, Cheonan, Korea.

Seungjun Kim
School of Civil, Environmental, and Architectural Engineering, Korea University, Seoul, Korea., rocksmell@korea.ac.kr

Internal Force Evaluation of a Submerged Floating Pipeline Under Irregular Waves

Acknowledgements

This study was supported by Korea Institute of Ocean Science and Technology (Grant/Award number: PE99832).

Journal of Marine Science and Technology, Vol. 28, No. 6, pp. 582-592 (2020)
DOI: 10.6119/JMST.202012_28(6).0013

INTERNAL FORCE EVALUATION OF A SUBMERGED FLOATING PIPELINE UNDER IRREGULAR WAVES

Deokhee Won[1], Jihye Seo[1], Jong Sup Park[2], and Seungjun Kim[3]

Key words: submerged floating pipeline, internal force, behavior, irregular waves.

ABSTRACT

Generally, submarine pipelines are laid on the seabed to transport water, oil, natural gas, and electricity to the land using submarine cables. However, they are not suitable for all seafloor conditions. There are environmental concerns such as deep seas, irregular seabed features, soft soils, transported materials and so on. To overcome these challenges, a submerged floating pipeline (SFP) concept was proposed. To stay in the middle of the water, the SFP has buoyant modules as floating devices. It is unrestricted under environments such as uneven seabeds, and deep waters, and is suspended to avoid interrupting passing vessels. This SFP model was applied in some parts of the water supply project from southern Turkey to Northern Cyprus in 2014. It was found that SFPs have advantages of application in various underwater environmental conditions. In this study, the internal forces of SFPs were evaluated under the irregular wave condition. The main parameters were set as the buoyancy to weight ratio, anchoring method of the tendon, suspended depth of the pipes, and incident angles of the wave. Consequently, the SFP was subjected to not only bending forces but also torsional forces. The sectional characteristics of the pipe were analyzed based on the results to conclude on the optimum design.

I. INTRODUCTION

On May 19, 2015, Refugio State Beach experienced an accidental crude oil release from its 24-inch underground pipeline named Line 901, built by the Plains All American Pipeline located in Santa Barbara County, California. This was because it originated from the land and then entered the ocean. Line 901, the severely corroded pipeline that failed in 2015, caused a large coastal oil spill. The Santa Barbara Coast had previously suffered a massive oil spill in 1969, which led to the designation of International Mother Earth Day. Additionally, offshore pipelines are facing stricter regulations for oil infrastructure and transport owing to recent oil spills such as Shell's pipeline at the North sea in 2011, the Oil and Natural Gas Corporation Ltd.'s pipeline at the Mumbai High Field in 2011, and Husky Energy's pipeline leaks at the SeaRose platform in Newfoundland Canada in 2018.

Although pipelines were considered as efficient means of transporting oil and gas, the conventional pipeline was constructed on the seabed using the pulling, floating and sinking, and lay barge methods. The uneven seafloor topography is the greatest limitation when installing conventional submarine pipelines, and the greatest risk is the oil leakage that pollutes the sea. Oil leakages not only pollute the sea but also the seabed soil. According to an outlook report (DNV-GL, 2019), the oil and gas industry will continue to play an important role and hydrocarbons will account for 44% of the total energy mix in 2050. There is growing pressure on the oil and gas industry to demonstrate its ability to continue delivering a secure and environmentally-sustainable supply of affordable energy. Moreover, there has been growing awareness on environmental protection, which has been reflected in the accelerating energy transition, driven largely by the electrification of the world's energy systems, and an increasing in decarbonized energy. Therefore, research studies on technically sophisticated and cost-effective energy concepts have been focused on the underwater pipeline design for oil and gas transportation in the offshore industry. Jeon et al. (2020) proposed a procedure to identify maneuvering coefficients that brought about abnormal motions in the simulation of a submerged body. Raheem, (2019) examined the behavior of lateral pipe-soil interaction placed on ultra-soft clayey soil. Additionally, in the authors' previous study (Kim et al., 2018; 2020), the behavior of a submerged floating pipeline (the following, SFP) under regular waves was analyzed based on the Northern Cyprus Water Supply Project. The SFP is an underwater suspended

Paper submitted 06/03/20; revised 11/18/20; accepted 12/05/20. Corresponding Author: Seungjun Kim (e-mail:rocksmell@korea.ac.kr)
[1] Coastal & Ocean Engineering Division, Korea Institute of Ocean Science and Technology, Busan, Korea.
[2] Department of Civil Engineering, Sangmyung University, Cheonan, Korea.
[3] School of Civil, Environmental, and Architectural Engineering, Korea University, Seoul, Korea.

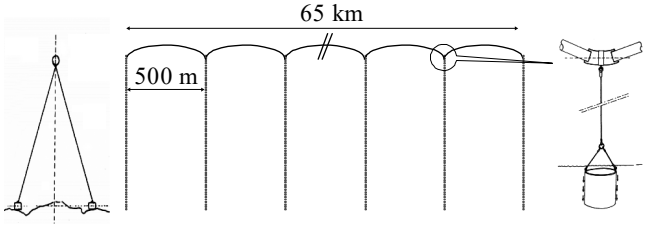

Fig. 1. Installation method of submerged floating pipeline (Kruijt, 2003)

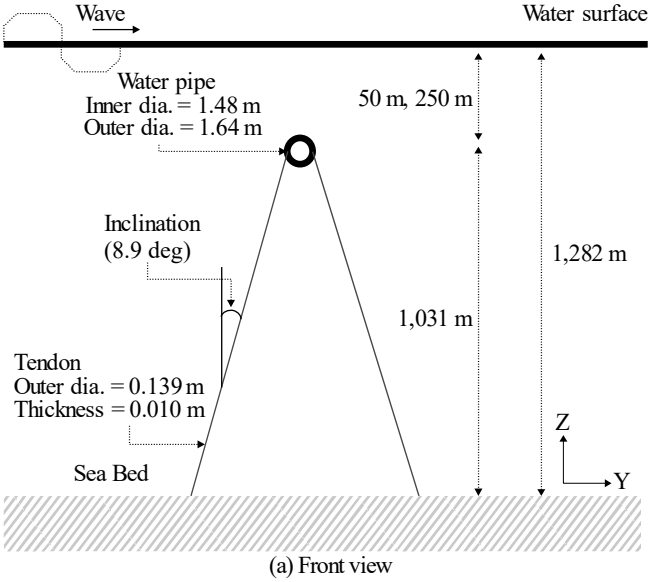

(a) Front view

(b) FE model

Fig. 2. Configuration of the SFP model

system that is installed in areas that do not affect ship navigations, and where the influence of wind driven waves on the water depth is low. It ensures economic feasibility in deep water depths, and has an eco-friendly advantage relative to the marine environment. It is also much easier to operate and maintain the detection and monitoring system that prevents the aforementioned pipeline oil spills.

SFPs are exposed to a very complex system of hydrodynamic reactions such as waves and currents. As shown in Fig. 1, they are composed of tendons supported at regular intervals by buoyancy units, or pipes made of buoyant material, and are flexible enough to endure external forces. The hydrodynamic behaviors of SFPs under irregular waves are evaluated in this study based on the variables obtained in the previous research (Kim et al., 2018; 2020) under regular waves in the Turkey-Cyprus project. In the present study, the hydrodynamic response of SFPs under irregular waves was analyzed using the commercial code ABAQUS-AQUA (Simulia, 2014), and the internal forces evaluated using design parameters.

II. ANALYSIS OUTLINE

1. Definition of Irregular Waves

The irregular waves acting on the SFP are regarded as the compound of a large number of small wave trains, each of which has its own length, height, and direction. The Joint North Sea Wave observation Project (JONSWAP) spectrum with fetch and wind speed parameters, proposed by Hasselman et al (1973) was considered for unidirectional irregular waves by the wave potential theory as the frequency spectrum, which is shown in Eq. 1 to Eq.4 (Goda, 2010). This spectrum is a modified form of the Pierson and Moskowitz (PM) spectrum (Pierson and Moskowitz, 1964) for fully developed seas, and has a sharp peak caused by an extra peak enhancement factor, indicating a marine environment with severe storms. It is expressed in terms of a significant height and peak period as follows.

$$S(f)=\beta_j H_s^2 T_p^{-4} f^{-5}\exp\left[-1.25(T_p f)^{-4}\right]\gamma^{\exp\left[-\frac{(T_p f-1)^2}{2\sigma^2}\right]} \quad (1)$$

in which

$$\beta_j \cong \frac{0.0624}{0.23+0.0336\gamma-0.185(1.9+\gamma)^{-1}}\left[1.094-0.01915\ln\gamma\right] \quad (2)$$

$$T_p \cong T_s / \left[1-0.132(\gamma+0.2)^{-0.559}\right] \quad (3)$$

$$\sigma=\begin{cases}\sigma_a=0.07 : f\le f_p\\ \sigma_b=0.09 : f>f_p\end{cases} \quad (4)$$

$$\gamma=1\sim 7(\text{mean}:3.3)$$

where H_s, T_s, T_p, and f are the significant wave height, significant wave period, peak period, and wave frequency respectively; σ represents the energy spreading over the frequency range selected, and γ is the peak enhancement factor, which indicates the maximum spectral density value of the PM spectrum to that of the JONSWAP spectrum.

Given the spectrum of the wave heights, the time series of

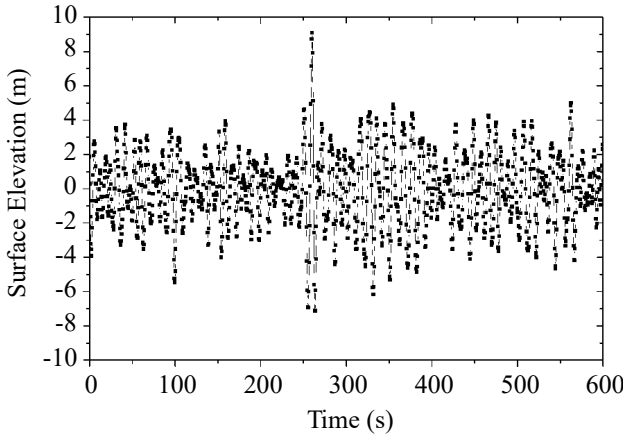

Fig. 3. Wave elevation time series.

the irregular waves with linear superposition can be generated as shown in Fig. 3. By applying the wave velocity potential to Morison's equation, the hydraulic force acting on the cylindrical structure at a specific position can be calculated over time (Kim et al., 2016). In this study, a wave elevation time series derived from the JONSWAP spectrum was compared with the time series reconstructed using FFT (Fast Fourier transform) from the discretized amplitude spectrum. The wave number was calculated from the linear wave dispersion, the discrete amplitude was determined using specific periods, and arbitrary phases were generated randomly. This can be considered as a reasonable input for the model under irregular waves.

2. Analysis Outline

To investigate the hydrodynamic characteristics of the SFP under irregular waves, the analysis model was assumed to be similar to the model in the comparative study (Kim et al., 2020), which evaluated the behavior of the SFP under regular waves. The environmental conditions and main properties are listed in Table 1. The SFP in the Northern Cyprus Water Supply Project covers a considerably long distance; therefore, the present analysis model considered only 2.5 km of the entire 65 km. Fig. 2(a) shows the cross section of the model. It was composed of a pipe and anchoring system with tendons as shown in Fig. 2(b). The pipe, having a diameter of 1.48 m, was assumed to be made of high-strength plastic.

For irregular wave conditions, the water depth, significant wave height, and period were 1,282 m, 8.4 m, and 10 s, respectively. To represent these sea conditions, the input spectrum was plotted using a peak enhancement factor of 3.3. From this, the discrete amplitudes were determined by 216 frequency components using the equal energy discretization method, and phases were randomly generated from 0 to 360 degrees. Fig. 3 displays a wave elevation time series of 600 seconds in total.

In this study, ABAQUS version 6.14 (Simulia, 2014) was used to perform the numerical analysis. As shown in Fig. 2(b), the pipes and tendons were modeled as three-dimensional beam and truss elements, respectively. The analysis techniques such as the boundary conditions were also similar to those in Kim et al. (2020). Both ends of the SFP were fixed postulated as the landfall connection. The y- and z-axes of the model had free displacement; however, the x-direction was not free, to prevent the model components from leaning. To evaluate the dynamic response of the structure, an implicit dynamic analysis under the wave loads was performed after static analysis. Additionally, two points were defined as Points A and B, representing the middle of the pipe, and the top end of the tendon, respectively as shown in Fig. 2(b). Here, the motions of the model can be described in terms of surge, sway, and heave, which represent translational motion along the x-, y-, and z-axes; the rotational motions about the same set of axes are roll, pitch, and yaw (Fig 4(b)). Fig. 3 is wave elevation time series. This wave was subjected four times in a row. The total analysis time was 3200 seconds.

We performed the parametric study considering the buoyancy to weight ratio (BWR), tendon anchoring method, suspended depth of the pipe, and incident angle of the wave. These variables are derived from the references related to the

Table 1. Environmental conditions and main properties.

Parameters (unit)	Values
1. Environmental conditions	
Water depth (*h, m*)	1,282
Significant Wave period (T_s, *s*)	10.0
Significant Wave height (H_s, *m*)	8.4
Peak enhancement factor (γ)	3.3
Current Speed(m/s)	0.1
2. Pipe	
Outer diameter (*m*)	1.64
Wall thickness (*m*)	0.08
Elastic modulus (GPa)	0.25
Density (kg/m^3)	960
Drag/added-mass coefficient	1.2/1.0
Suspended depth (*m*)	50.0, 250.0
3. Tendon	
Outer diameter/thickness (*m*)	0.139/0.10
Elastic modulus (GPa)	210.0
Minimum yield stress (MPa)	482.6 (API X70)
Minimum ultimate stress (MPa)	565.4 (API X70)
Drag/added-mass coefficient	1.2/1.0
Tendon spacing (*m*)	500.0

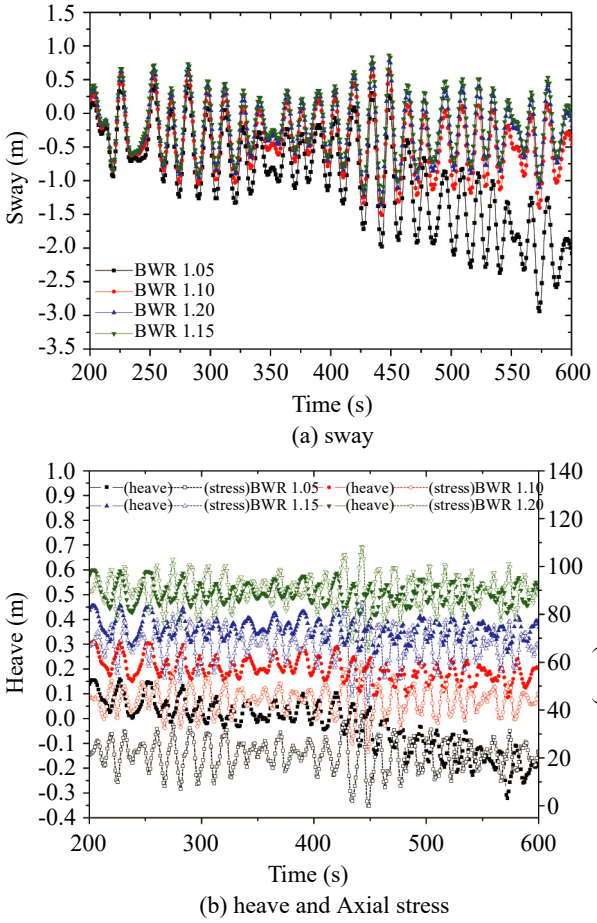

Fig. 4. Tendon motions and stress of the SFP according to BWR at Point B (T_s= 10 s, H_s= 8.4 m, and suspended depth = 50 m).

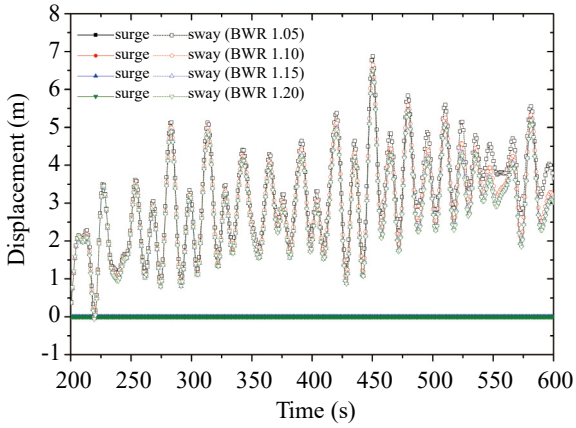

Fig. 5. Pipe motions of the SFP according to BWR at Point A (T_s = 10 s, H_s = 8.4 m, and suspended depth = 50 m).

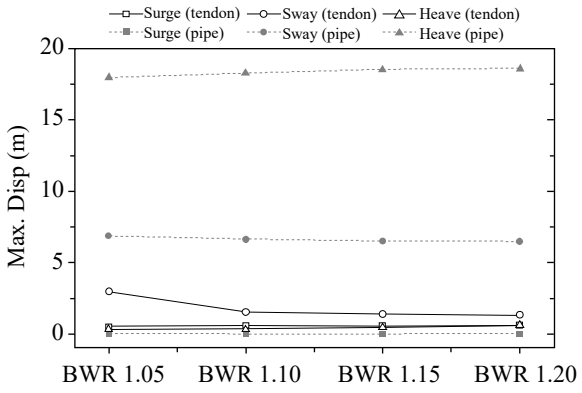

Fig. 6. Absolute maximum displacement according to BWR.

submerged floating tunnel for supporting (Cifuentes et al., 2015, Jin and Kim 2017, Yang et al., 2020) and described in the following sections, and the analysis results are compared with the previous results in Kim et al. (2020).

III. CHARACTERISTICS OF TENSION AND MOTION RESPONSE OF SFP

1. BWR

First, the behavior of the SFPs was analyzed using BWR ranging from 1.05 to 1.20. The BWR determines the amount of pre-tensions in the tendons. At 1.0, which is the no pre-tension state, a compressive force by the wave forces might occur in the tendon. Therefore, to guarantee tension in the tendons, and maintain the structural stability of the SFP, the BWR was set to greater than 1.0. The SFP controlled its buoyancy by the installation of a floating unit that connects the pipe and tendons. Here, the suspended depth of the pipes was set as 50 m.

Fig. 4 to Fig. 6 show the motion of the SFP at Points B and A, as well as the tension of the tendon according to the BWR under the irregular waves in Fig. 3. Although total analysis time was 3200 seconds, behavior of pipeline had same tendency after 600 seconds. Therefore, graphs of time series results were illustrated until 600 seconds.

First, Fig. 4 plots the tendon motions at Point B. The linear longitudinal motion (surge) and linear transverse motion (sway) are generated by the exertion of the wave forces on the SFP, and the linear vertical motion (heave) is caused by an uplifting force caused by the BWR. The sway of the tendon was decreased with the increase of the BWR of the SFP as shown in Fig. 4(a). The left axis in Fig. 4(b) shows the heave at Point B of the tendon. It can be observed that the uplifting force by the BWR increased the initial vertical movement and initial tension, and controlled the deformation of the tendon. This implies that the initial tension of the tendon restrains the deformation generated, as the buoyancy of the SFP increases. For suspension in the middle of water, the SFP is supported by buoyancy that is greater than the self-weight. This BWR determines the magnitude of the initial tension, and the motion of the SFP subjected to the dynamic load is induced, changing the tension of the tendon. The right axis in Fig. 4(b) also exhibits variations of the initial tension (open shape). It can be observed that the axial stress of the tendon increased proportionally as the BWR increased.

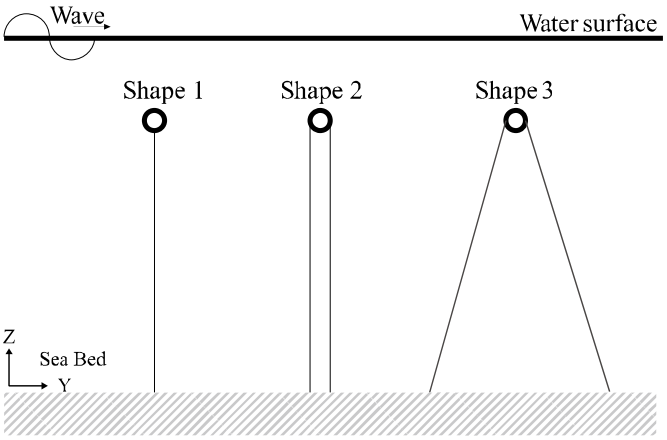

Fig. 7. Tendon anchoring method.

Next, Fig. 5 shows the pipe motion of the SFP according to the BWR. It represents the longitudinal and transverse displacement of the pipe at Point A, which is located in the middle of the pipe span. For the surge, the pipe was stable without the slightest reaction. The sway occurred for approximately 0 m to 7 m horizontally.

Finally, Fig. 6 illustrates the absolute maximum motion value of the tendon and pipe. Here, the open and close shapes represent the tendon and pipe motion, respectively. There were no significant variations with the BWR; however, the sway of the tendon was decreased slightly as the BWR increased. It can be deduced that this behavior pattern is similar to that of the regular wave condition. Whereas the maximum value of the tendon motion in the comparative study (Kim et al., 2020) was approximately 6 m, the maximum displacement of the tendon under irregular waves was approximately 3 m. It can be observed that the value reduced approximately twice compared to the case in the regular wave condition. For reference, the pipes of SFPs with an arched shape have an initial height of 14 m between the tendons, and can generate vertical deflection of up to 28 m. For the pipe motion under regular waves, the sway was 4 to 8 m, and the heave was approximately 25 m.

2. Tendon Anchoring Method

As a second parameter, different dynamic behaviors related to the supporting method of the tendon were evaluated. Fig. 7 shows three types of tendon anchoring for displacement control, which include Shape 1, Shape 2, and Shape 3 (as default). The SFP was controlled by one vertical tendon, two vertical tendons, and two oblique tendons with an inclination of 8.9°, respectively.

Fig. 8 to Fig 10 display the motion of the pipes and tendons as well as the stress of the tendon of the SFP under irregular waves, according to the anchoring method. Here, a BWR of 1.2 was applied as the common condition. First, Fig 8 illustrates the tendon motion and stress of the SFP at Point B, according to the anchoring method. It can be observed that

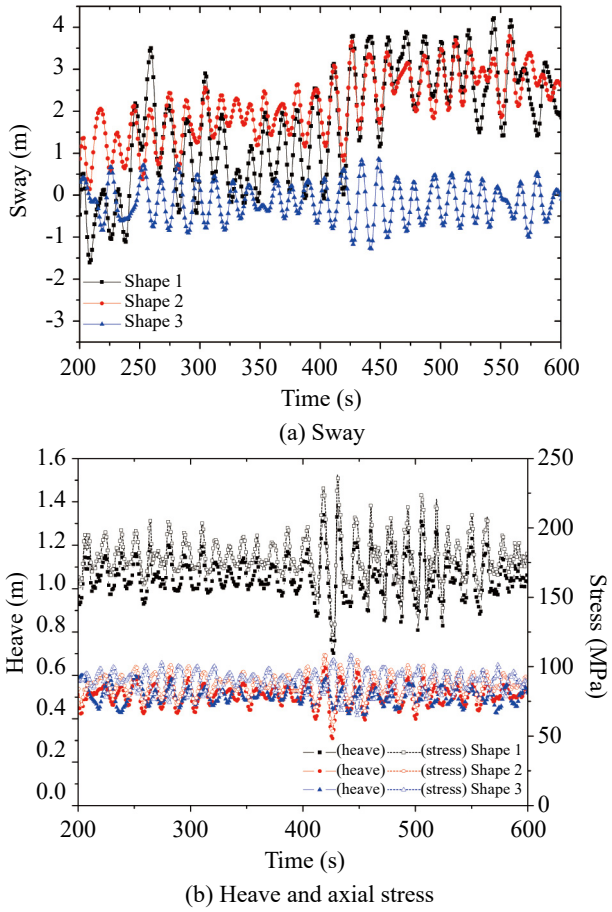

Fig. 8. Tendon motions and stress of the SFP according to the anchoring method at Point B (T_s = 10 s, H_s = 8.4 m, BWR = 1.2, and suspended depth = 50 m).

Shape 1 had the largest heave, and Shapes 1 and 2 had larger sways than Shape 3. Conversely, in the regular wave condition, the largest motion was generated in Shape 1 for both the sway and heave.

The right axis of Fig 8(b) shows the tendon stress of the SFP according to the anchoring method. After the formation of an initial stress by a BWR of 1.2, the variation occurred by the action of the irregular waves. The values of the initial tension are 140 MPa for Shape 1, and 100 MPa for Shapes 2 and 3. For Shape 1, the initial tension acts more than twice as much as in the other shapes. This is because it supports the upward force with one tendon under the same BWR condition. The developed stress of the tendon was lower than the allowable stress of 482.6 MPa stated in the material properties (Table 1). This was by approximately 50%, which can be considered safe.

Finally, Fig. 9 displays the pipe motion of the SFP at Point A, according to the anchoring method. Like the tendon motion, there was a slight surge according to the parameter. As shown in Fig. 9(a) and Fig. 9(b), the difference in the tendon number also influences the sway and heave of the pipe. Additionally, it was found that Shape 3 with the oblique angle, exhibits the best performance in motion control, among the suggested

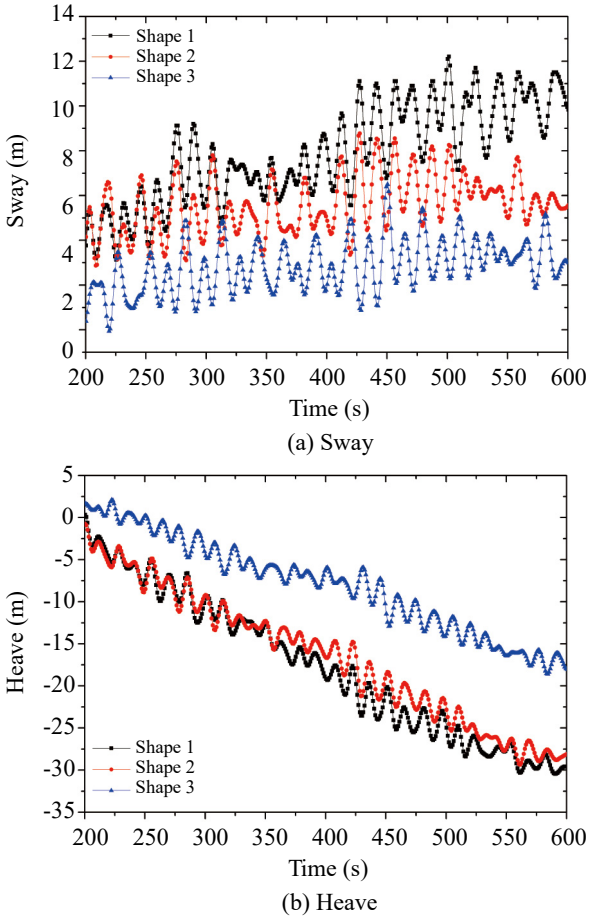

Fig. 9. Pipe motions of the SFP according to the anchoring method at Point A (T_s = 10 s, H_s = 8.4 m, BWR =1.2, and suspended depth = 50 m).

methods as shown in Fig.10. Additionally, compared to the fact that the maximum tendon sway of Shape 2 was approximately 8 m under the regular waves (Kim et al., 2020), it showed a reduction of approximately two times in the maximum tendon sway, owing to the influence of the irregular waves. Moreover, the pipe motions also showed that Shape 3 had the best performance. The maximum sway of Shape 1 was reduced to approximately 30 m for the irregular waves, whereas the maximum sway was approximately 40 m for the case under regular waves.

3. Suspended Depth of SFPs

We considered the suspended depth of the SFPs as the third parameter, which indicates the clearance between the water surface and the top of the pipes; it represents the installation depth of the pipes. The SFP in the Northern Cyprus Water Supply Project was installed at a depth of 250 m; the suspended depths of the SFPs in this study were set as 50 m (shallow water) and 250 m (deep water).

Fig. 11 to Fig 13 show the motion of the pipes and tendons as well as the tendon stress of the SFPs under irregular waves

Table 2. Axial stress of the tendon according to the suspended depth.

Wave condition	Depth	Values
Regular	250 m	Max. 68 MPa
	50 m	Fluctuation Max. 15 MPa
Irregular	250 m	Max. 90 MPa
	50 m	Fluctuation Max. 30 MPa

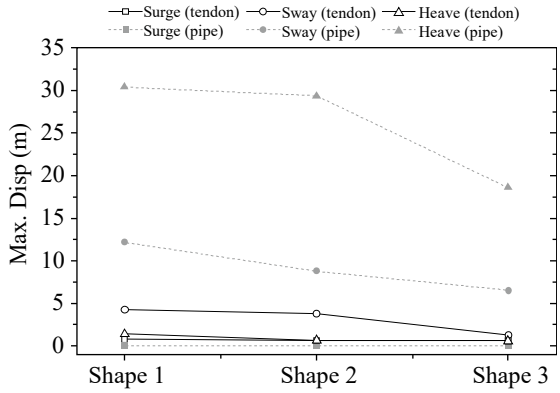

Fig. 10. Absolute maximum displacement according to the anchoring method.

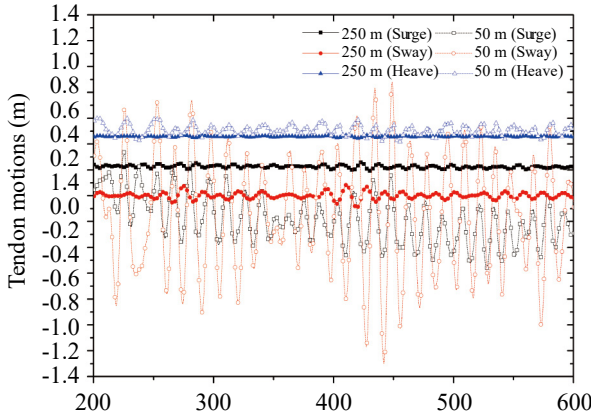

Fig. 11. Tendon motions of the SFP according to the suspended depth at Point B (T_s = 10 s, H_s = 8.4 m, and BWR = 1.2).

based on the suspended depth. First, Fig 11 illustrates the tendon motion of the SFP at Point B, the uppermost part of the tendon. It was found that deformations caused by the irregular waves rarely occurred at the depth of 250 m. This is because the influence of the waves decreases as the fluid particles move vertically away from the free water surface by the orbital motion of the waves in deep water. In the shallow water, the waves were significantly affected by the sea bottom topography.

Next, the tendon stress of the SFP according to the suspended depth was summarized in Table 2 and compared with

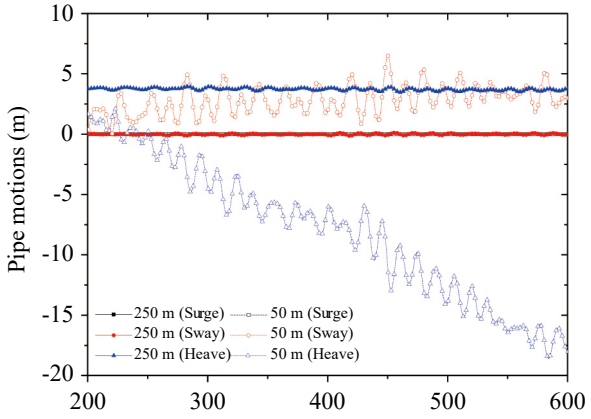

Fig. 12. Pipe motions of the SFP according to the suspended depth at Point A (T_s = 10 s, H_s = 8.4 m, and BWR = 1.2).

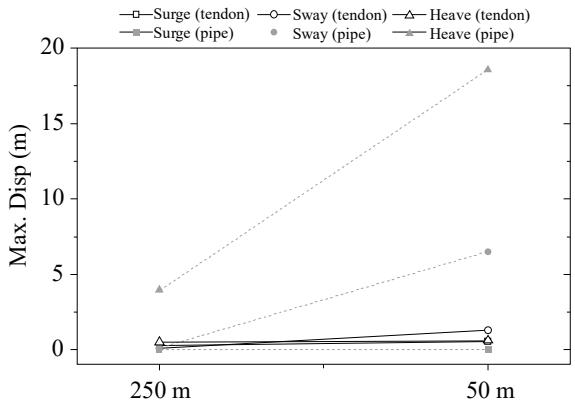

Fig. 13. Absolute maximum displacement according to the suspended depth

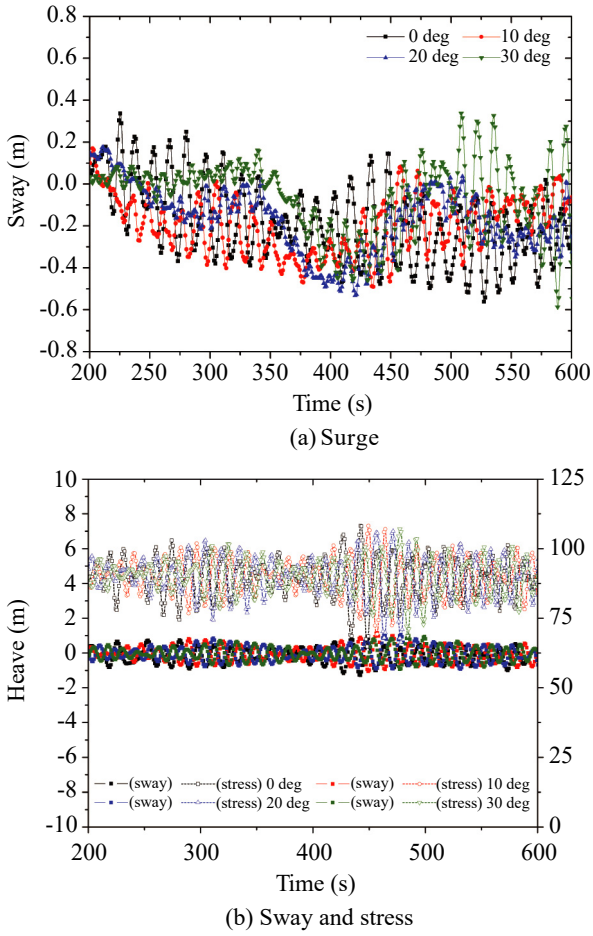

Fig. 14. Tendon motions and stress of the SFP according to the incident angle at Point B (T_s = 10 s, H_s = 8.4 m, BWR = 1.2, and suspended depth = 50 m).

the regular wave condition. It can be observed that tendon stress of approximately 90 MPa occurred in the 250 m-depth model and was slightly changed, whereas in the 50 m-depth model, it fluctuated to a maximum range of 30 MPa. Compared to the regular wave condition (Kim et al., 2020), which had a stress fluctuation of approximately 15 MPa in the 50 m-depth model, and a constant value of approximately 68 MPa in the 250 m-depth model, it was confirmed that the tendon motion had a similar pattern based on the water depth for both wave conditions. However, there was a quantitative difference in the tendon stress under the irregular waves.

Next, Fig. 12 plots the pipe motion of the SFP at Point A according to the suspended depth. For the deep water case, there were slight changes in the tendon motion as shown in Fig 12. For the heave of the pipe, the blue line shows the vertical deformation of the pipe related with the suspended depth. While it can be observed that the initial buoyancy by BWR continued in the 250 m-depth model, the heave in the 50 m-depth model decreased steadily under the irregular waves.

Lastly, Fig. 13 plots the absolute maximum motion value of the tendon and pipe. It can be observed that the maximum displacement of the tendons was approximately 1.3 m of sway at the 50 m-depth, and 0.5 m of heave at the 250 m-depth; the maximum displacement of the pipes was 18.6 m and 3.9 m of heave at the 50 m- and 250-m depth, respectively. In the comparative study (Kim et al., 2020), it was found that the maximum tendon displacement in the regular wave condition was approximately 2.3 m of sway in the shallow water case, and 0.5 m of heave in the deep water case. For the maximum pipe displacement, it was approximately 27.5 m and 4.9 m of heave in the shallow, and deep water cases, respectively. It was verified again that the influence of the wave in the case of the deep sea was decreased. These also did not vary significantly from the behavior pattern of the pipe in the regular wave condition; however, it was found that the absolute maximum displacement in the shallow sea had a slightly smaller value than that of the regular wave condition.

4. Wave Incident Angle

The last parameter is the angle of incidence, which was varied from 0 to 30 degrees at intervals of 10 degrees. Here, it denotes the angle between the wave propagation direction and

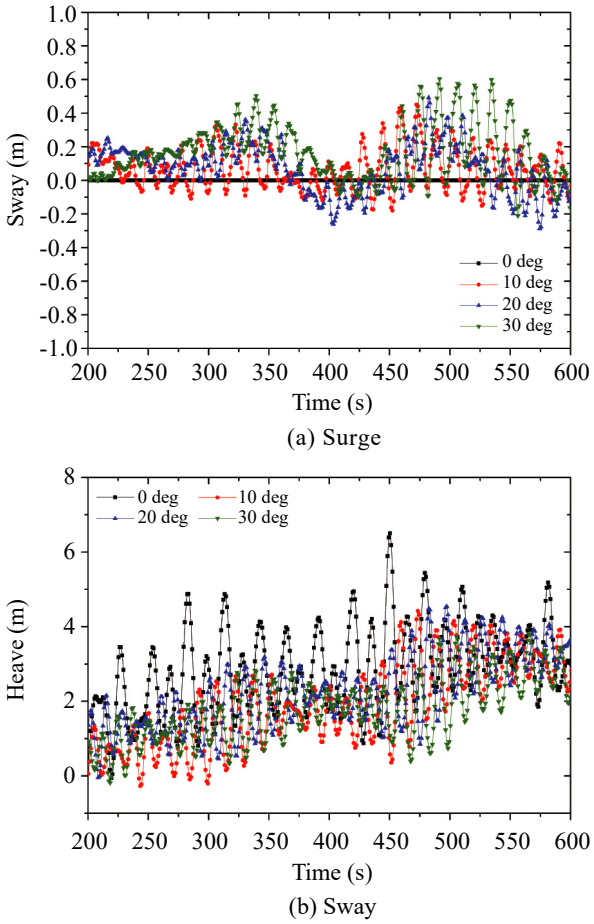

Fig. 15. Pipe motions of the SFP according to the incident angle at Point A (T_s = 10 s, H_s = 8.4 m, BWR = 1.2, and suspended depth = 50 m).

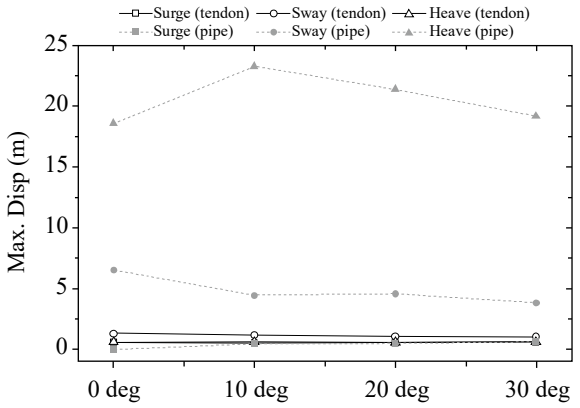

Fig. 16. Absolute maximum displacement according to the incident angle.

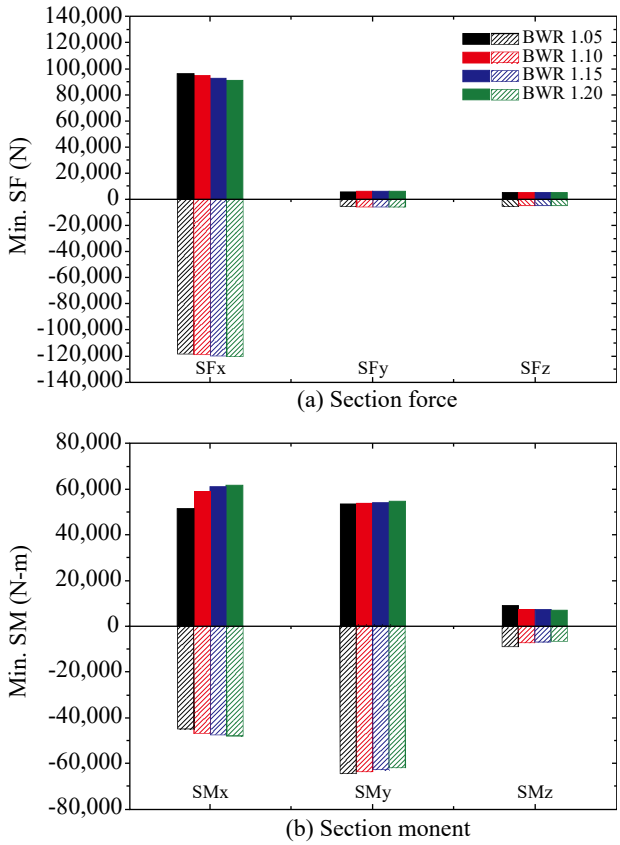

Fig. 17. Section force and moment of pipe according to BWR (T_s = 10 s, H_s = 8.4 m, and suspended depth = 50 m).

the normal to the SFP. In this study, unidirectional irregular waves were exerted to the SFP, considering the frequency spectrum only, and not the direction spectrum. However, the primary wave direction in actual seas changes depending on the season and marine environment conditions. Therefore, behavior analysis was performed using the angle of incidence as a variable. The common conditions were BWR = 1.2, and the suspended depth of the pipes was set as 50 m.

Fig. 14 to Fig 16 illustrate the motion of the pipes and tendons as well as the stress of the SFP under irregular waves according to the wave incident angle. First, Fig. 14 exhibits the tendon motion and stress of the SFP according to the incident angle. For the regular wave condition, it was inferred that the surge in the tangential direction of the SFP was generated continuously in the 10 and 20 degree models, which may cause the torsion of the SFP. However, for the irregular wave condition as shown in Fig. 14(a), it can be observed that the maximum value of the surge was similar for all the angles, and the influence of the incident angle had less impact on the tangential deformation. The right axis in Fig.14(b) shows the tendon stress of the models according to the incident angle. Because the analysis models with a BWR of 1.2 were stable in the displacement control, there are no significant deformations. It can be observed that the tendon stress increases as the sway increases owing to the superposition of the waves.

Next, Fig. 15 shows the pipe motion of the models at Point A according to the incident angel. For Fig. 15(a), as the angle of incidence increased, the pipe generated a large surge; however, there was little deformation in the 0 degree-model. Additionally, as shown in Fig. 15(b), the sway of the

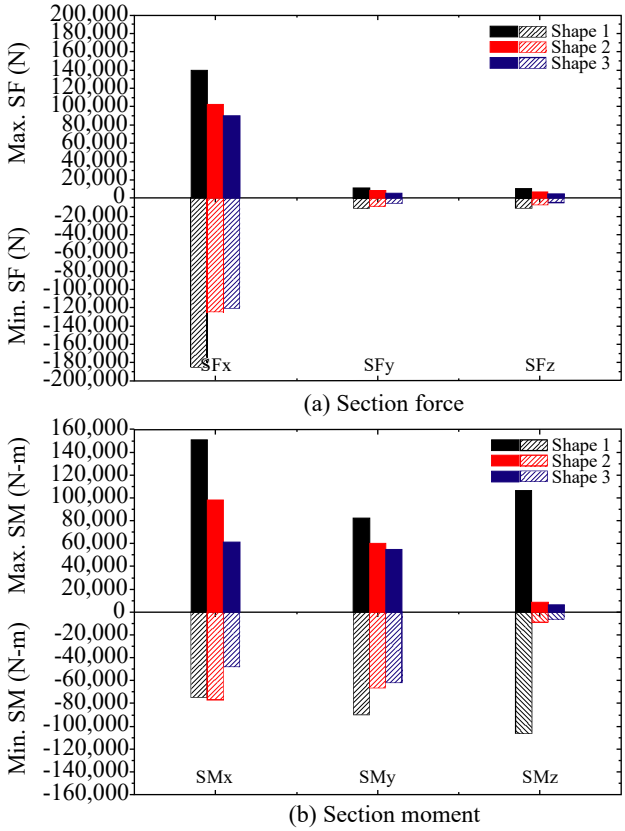

Fig. 18. Section force and moment of the pipe according to the anchoring method (T_s = 10 s, H_s = 8.4 m, BWR = 1.2, and suspended depth = 50 m)

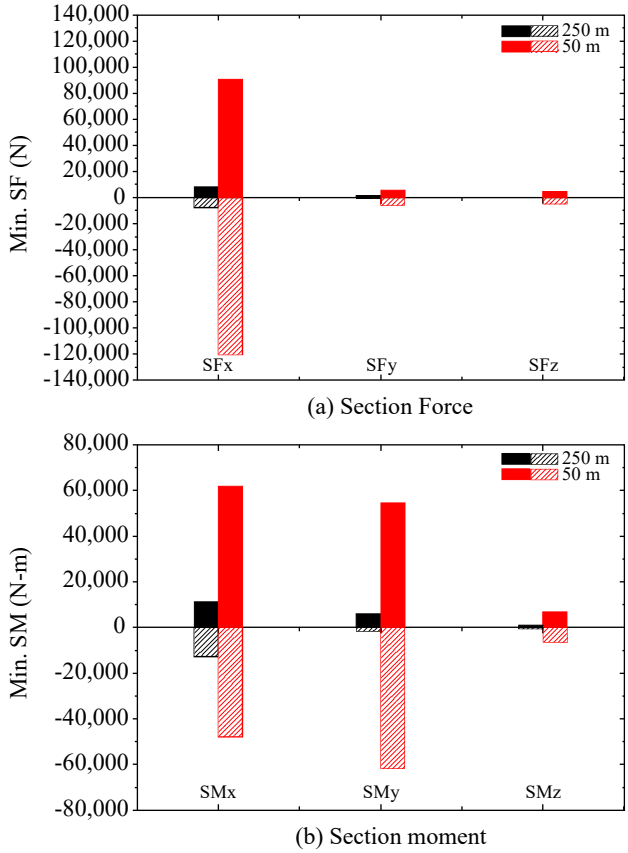

Fig. 19. Section force and moment of the pipe according to the suspended depth (T_s = 10 s, H_s = 8.4 m, and BWR = 1.2).

pipes was less influenced by the incident angle compared to that of the regular wave condition. The heave had a similar pattern to that of the regular wave condition; however, its deformation for each arbitrary wave period was significantly fluctuated.

Lastly, Fig. 16 plots the absolute maximum motion value of the tendon and pipe. When comparing the absolute maximum displacement, it can be confirmed that the influence of the incident angle was less than that of the regular wave condition. Further, it was observed that these results had a slightly smaller value than that of the regular wave condition.

IV. CROSS-SECTIONAL CHARACTERISTICS OF SFP

Pipelines as well as SFPs are not installed in a completely straight line at sea. Owing to the external forces and boundary conditions, the sectional characteristics of SFPs continuously vary according to the wave loads. Therefore, for the design of SFPs, it is necessary to examine the internal forces of the pipe. This section describes the static response of pipes according to the major design parameters. Here, the inside of the pipe was assumed to be empty, which means there was no water flowing through it, and no internal pressure such as hoop stress pushing against the edges of the pipe walls. The cross-sectional characteristics of the pipe were derived based on this, and analyzed according to the four variables as follows.

1. BWR

The first variable for the design is the BWR of the SFPs. The section force and moment of the pipe according to the BWR was analyzed as shown in Fig. 17(a) and Fig. 17(b), respectively. Here, the x-axis section force, SFx represents the axial force in the surge-direction of the model, the y-axis section force, SFy is the shear force in the sway-direction, which had the greatest variation at both node ends, and the z-axis sectional force, SFz is the shear force in the heave-direction. Additionally, SMx, SMy, and SMz represent the section moment in the roll, pitch, and yaw directions, respectively. The solid columns represent the maximum compression force and moment, and the patterned ones represent the maximum tensile force and moment.

It was observed that the axial force in the surge-direction of the pipe was the largest as shown in Fig. 17(a), and was generated in the middle of the SFP. The pipe was under tensile and compressive forces of approximately 96,000 N and 120,000 N, respectively. The shear forces had relatively small sectional forces of 6,100 N or less. Regarding the section

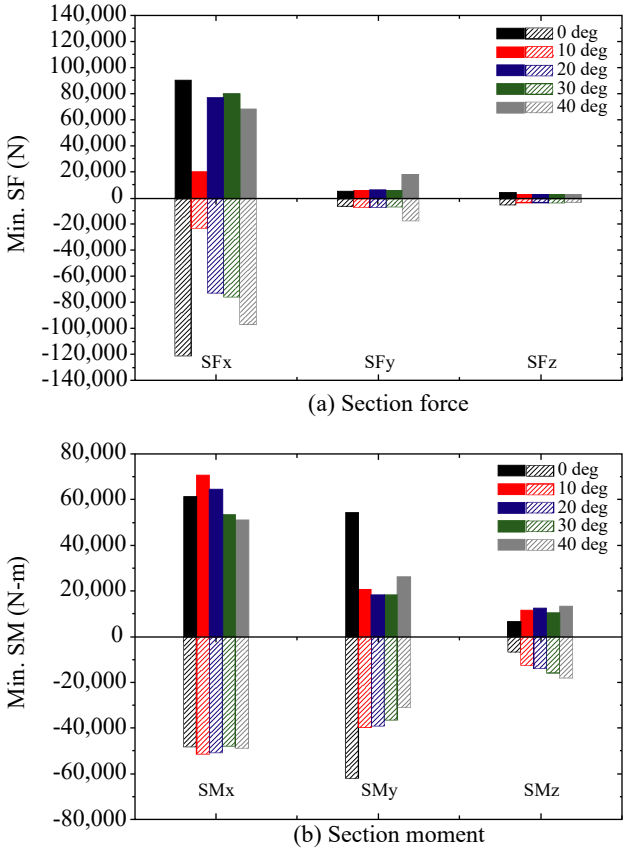

Fig. 20. Pipe motions of the SFP according to the incident angle method (T_s= 10 s, H_s= 8.4 m, BWR=1.2, and suspended depth=50 m).

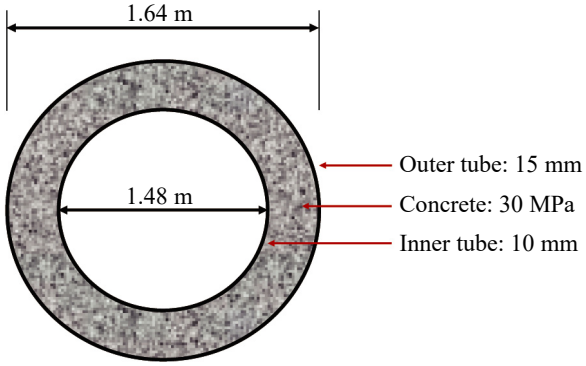

Fig. 21. Cross-section dimension of the pipe

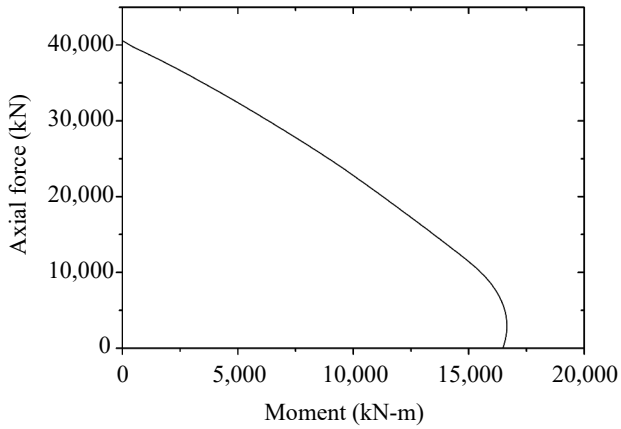

Fig. 22. P-M interaction curve

moment in Fig. 17(b), the pitch-direction in the y-axis of the pipe generated the largest negative moment, which was larger than that of the regular wave case, but had less impact on the BWR. For reference, it was confirmed in the previous study (Kim et al., 2020) that the maximum positive section moment was generated at the joint nodes with tendons and pipes, and the maximum negative section moment was generated at the middle support point.

2. Tendon Anchoring Method

The second variable for the section design of the SFPs is the tendon anchoring method. Fig. 18 shows the section force and moment of the SFP according to the anchoring methods in Fig. 7. As with the hydrodynamic analysis, Shape 3 had the best performance as shown in Fig 18(a). The characteristics were similar to those in the regular wave case, where the axial force was predominant. Additionally, the generated section moment related with the anchoring method was larger than that of other parameters as shown in Fig. 18(b). This may be because the pipe motions of Shapes 1 and 2 were larger as shown in Fig. 9.

3. Suspended Depth of SFPs

This section presents the sectional characteristics of the SFPs according to the suspended depth as the third variable for the sector design. Fig. 19 illustrates the section force and moment of the SFP according to the suspended depth. It can be observed that the section force and moment were hardly generated in the 250 m-model similar to the pipe motion behavior in Fig. 12. However, the negative moment in the pitch-direction of the 50 m-model was larger than that of the comparative study.

4. Wave Incident Angle

The last variable for the section design is the incident angle of the waves. As mentioned in Section III.4, because unidirectional irregular waves were exerted to the SFP in this study, the incident angle was varied from 0° to 40°and analyzed.

Fig. 20 shows the section force and moment of the pipe according to the wave incident angle. This also showed similar behavior to the cross-section characteristics in the third parameter, the suspended depth of the SFP. For the section force in Fig. 20(a), it was observed that the axial force of the pipe was predominantly affected for all angles of incidence. The section moment in Fig. 20(b), except for SFz, was to be dominant along the pitch-and roll direction.

V. DESIGN OF SFP SECTION

Summarizing the above analysis, the cross-section of the

SFPs should be adequately resistant to the axial forces, bending moments, and torsional moments. In this study, the cross-section of the pipe was designed using a double-skinned composite tubular (DSCT) section as shown in Fig. 21. The DSCT section is filled with concrete between the inner and outer tubes, and has excellent performance. As shown in Fig. 21, the pipe has outer and inner diameters of 1.64 m and 1.48 m, respectively. The outer and inner tubes, which are made of steel, have thicknesses of 15 mm and 10 mm, respectively. The material properties of the steel were an allowable stress of 240 MPa, tensile stress of 400 MPa, elastic modulus of 210 GPa, and Poisson's ratio of 0.3. For the concrete, a compressive strength of 30 MPa was applied.

Fig. 22 shows the P-M interaction curve of this section. The compression and moment performances of the section were analyzed. According to the curve, the cross-section of the pipe had a compressive force of 40,000 kN, and moment performance of 16,000 kN-m. In comparison with the cross-sectional characteristics in Section IV, it can be inferred that the distribution was within 5% of the maximum moment and axial forces under all the variable conditions.

VI. CONCLUSIONS

In this study, the hydrodynamic and cross-sectional characteristics of SFPs under irregular waves were evaluated based on four parameters: BWR, tendon anchoring methods, suspended depths, and wave incident angles. Moreover, internal forces(moments) should evaluate for design of pipeline section. Hence, a new type pipeline section was designed using section force and moment considered of hydrodynamic effect. We might get optimal section of submerged floating pipeline through proposed analysis procedures. In addition, designed DSCT section needs detail evaluation and optimal joint of modules to apply on the offshore fields.

ACKNOWLEDGEMENTS

This study was supported by Korea Institute of Ocean Science and Technology (Grant/Award number: PE99832).

REFERENCES

Cifuentes, C., S. Kim, M. H. Kim and W. S. Park(2015). Numerical simulation of the coupled dynamic response of a submerged floating tunnel with mooring lines in regular waves. Ocean Systems Engineering 5(2), 109-123.

DNV GL. (2019). Energy Transition Outlook 2019: Oil and Gas, A global and regional forecast to 2050

Goda, Y. (2010). Random seas and design of maritime structures (Vol. 33). World Scientific Publishing Company.

Hasselmann K., T.P. Barnett, E. Bouws, H. Carlson, D.E. Cartwright, K. Enke, J.A. Ewing, H. Gienapp, D.E. Hasselmann, P. Kruseman, A. Meerburg, P. Mller, D.J. Olbers, K. Richter, W. Sell and H. Walden.(1973). Measurements of wind-wave growth and swell decay during the Joint North Sea Wave Project (JONSWAP)' Ergnzungsheft zur Deutschen Hydrographischen Zeitschrift Reihe, A(8) (Nr. 12), p.95.

Jeon, M.J., T. T. Nguyen, H. K. Yoon and H. J. Cho (2020). A study on verification of the dynamic modeling for a submerged body based on numerical simulation. International Journal of Engineering and Technology Innovation 10(2), 107.

Jin, C. and M. Kim (2017). Dynamic and structural responses of a submerged floating tunnel under extreme wave conditions. Ocean Systems Engineering 7(4), 413-433.

Kim, S., W.S. Park and D.H. Won (2016). Hydrodynamic analysis of submerged floating tunnel structures by finite element analysis, Journal of Korean Society of Civil Engineers, KSCE 36(6), 955-967 (in Korean).

Kim, S.J., J. Seo and D.H. Won (2018). Hydrodynamic analysis of submerged floating pipeline under regular wave. Journal of Korean Society of Steel Construction 30(6), 335-345 (in Korean).

Kim, S.J., D.H. Won,, J.H. Seo, W. M. Jeong and Y. J. Kang (2020). Hydrodynamic behavior of submerged floating pipeline under regular waves. Journal of Pipeline Systems Engineering and Practice 11(3), 04020017.

Kruijt, N. (2003). Turkey-Cyprus submerged floating freshwater pipeline, Delft University of Technology, Netherlands.

Pierson, W.J. and L. Moskowitz (1964) A proposed spectral form for fully developed wind seas based on the similarity theory of S.A. Kitaigorodskii, Journal of Geophysical Research 69(24), 5181-5190.

Raheem, A. M. (2019). On the behavior of lateral pipe-soil interaction in ultra-soft clayey soil using large scale-laboratory tests. International Journal of Engineering and Technology Innovation 9(2), 119.

Simulia, lnc. (2014). ABAQUS 6.14 User's Manual. Dassault Systems, Providence, RI, USA, 2014.

Yang, Z., J. Li, H. Zhang, C. Yuan and H. Yang (2020). Experimental study on 2D motion characteristics of submerged floating tunnel in waves. Journal of Marine Science and Engineering 8(2), 123.